Deciphering the mechanistic insights of 4-nitrophenol reduction catalyzed by 1D-2D Bi$_2$S$_3$ nanostructured catalyst

Bhagirath Mahto, Ashok Barhoi, Haider Ali and Sahid Hussain*

Department of Chemistry, Indian Institute of Technology Patna, Bihta, 801103

Email: sahid@iitp.ac.in; Phone: +91-6115-233022

Text S1. Materials

Bismuth (III) nitrate pentahydrate (Bi(NO$_3$)$_3$·5H$_2$O, >98%) and thiourea (>99%) were purchased from the Central Drug House (P) Ltd. (New Delhi, India) and Tokyo Chemical Industry Co. Ltd. (Tokyo, Japan) respectively. Sodium borohydride (99%), deuterated sodium borohydride (98 atom % D), and deuterium oxide (99.9 atom % D) were purchased from Sigma-Aldrich. 4-Nitrophenol (99%), polyvinylpyrrolidone (average mol wt. 40,000), and 3-nitrophenol (>98%) were purchased from Alfa Aesar. 2-Nitrophenol (> 99) was purchased from Sisco Research Laboratories (SRL) Pvt. Ltd. - India. Ethanol was purchased from Merck. The chemicals mentioned above are used directly without further purification.

Text S2. Catalysts characterization

Powder X-ray diffraction (P-XRD) data were recorded in the 2θ range of 10-80° at a step of 0.02° on a PANalytical X-ray diffractometer with Cu Kα (λ = 1.5406 Å) radiation having tube voltage 45 kV and tube current 40 mA. The phases of as-synthesized materials were identified using the Joint Committee on Powder Diffraction Standards (JCPDS) database. A Perkin Elmer spectrum 400 FT-IR (Fourier transform infrared) spectrophotometer (United States) was used for FTIR measurements in the KBr pellets mode with the number of scans 32 in the wavenumber range

4000–400 cm^{-1} with a resolution of 4 cm^{-1}. Quantachrome Autosorb iQ_2 specific surface analyzer was used to test the samples' specific surface area, pore size, and pore volume at 77 K using N_2 adsorption-desorption isotherm. Prior to the measurements, the sample was degassed under a vacuum for 6 hours at 90 °C. The Brunauer-Emmett-Teller (BET) specific surface area was calculated from the adsorption data in the relative pressure (P/P_0) range from 0.05 to 0.35. Pore size distribution was estimated using Barrett–Joyner–Halenda (BJH) method using desorption branch of N_2 isotherm. Thermogravimetric analysis (TGA) was performed on an SDT Q600 instrument with a controlled heating rate of 10 °C/min in an N_2 environment from room temperature to 800 °C. The reduction properties of the 1D-2D Bi_2S_3 were evaluated by the temperature-programmed reduction (TPR, Quantachrome, TPRwin v3.52, USA) equipped with a thermal conductivity detector (TCD). Approximately 60 mg of material was used for the TPR study. The temperature was raised from ambient to 800 °C at 10 °C min^{-1} under a flow rate of 50 ml min^{-1} of H_2 (10%)/Ar. Diffuse reflectance spectroscopy (DRS) was recorded with a UV–vis spectrophotometer (Shimadzu UV2600) using $BaSO_4$ as a reflectance standard. Dynamic light scattering (DLS) analysis for hydrodynamic diameter was measured by Litesizer 500 particle analyzer from Anton Paar. The field emission scanning electron microscopy (FE-SEM) micrographs were obtained using a Zeiss Gemini SEM500 instrument coupled with an energy dispersive spectroscopy (EDS) detector. The transmission electron microscopy (TEM) and high-resolution TEM (HR-TEM) micrographs were obtained using a JEOL JEM 200 electron microscope at an acceleration voltage of 200 kV. The powder material was dispersed in ethanol, and then a drop of the suspension was deposited on the carbon film of the 200 nm mesh copper grids and then dried overnight. Finally, the UV-visible (UV–Vis) spectra were obtained using a spectrophotometer (Shimadzu UV2550) to study the catalytic reduction of 4-nitrophenol.

Text S3. Fabrication of Bi$_2$S$_3$ electrode

Firstly, the 5 mm glassy carbon electrode (GCE) is cleaned with 0.05 µm alumina slurry using a polishing kit, followed by rinsing with ethanol and deionized water and drying overnight at room temperature. To create the catalyst ink for making the working electrode, a mixture is prepared by combining 5 mg of Bi$_2$S$_3$ with 0.5 ml of ethanol and adding 10 µl of a 5 wt% Nafion solution to act as a binder. This mixture is then subjected to sonication until it becomes uniformly blended. Further, 10 µl of Bi$_2$S$_3$ ink was drop cast on the precleaned GCE to fabricate the Bi$_2$S$_3$ working electrode and dried overnight at 40 °C. Bi$_2$S$_3$/GCE was used for the electrochemical study of the mechanism of 4-NP reduction.

Text S4. Large scale catalytic reduction of 4-NP

Typically, 4-NP is present in industrial wastewater at a significant level, with concentrations usually exceeding 2 g·L^{-1} (equivalent to about 14.38 mM). To assess the effectiveness of the catalysts in treating wastewater containing high concentration of 4-NP, experiments were conducted using higher concentrations of 4-NP. Initially, a glass vial was filled with 10 ml of a 4-NP solution with a concentration of 15 mM. While stirring continuously, 60 mg of NaBH$_4$ was introduced into the solution, followed by adding 10 mg of catalyst. The UV-Vis absorption spectroscopic measurement was used to confirm the completion of the reaction. To ensure the presence of the reduced product 4-AP, a cuvette was filled with 200 µl of the reduced solution and 2.3 ml of deionized water, and the UV-Vis spectrum was measured.

Text S5. Large scale synthesis of 4-NP for spectroscopic measurements

To obtain more reduction products of 4-AP for spectroscopic measurements, a large-scale synthesis was performed following the procedures described below. Initially, 15 mg of 4-NP was dissolved in 3 mL of water under magnetic stirring in a glass vial. Following this, 10 mg of the

catalyst was added. Next, 30.0 mg of solid $NaBH_4$ was promptly introduced into the reaction container. Once the reaction was finished, its completion was confirmed using UV-Vis absorption spectroscopy, where the characteristic peak of 4-NP at approximately 400 nm vanished. Subsequently, the solution was extracted three times with 5 mL of ethyl acetate, and the products present in the organic phase were collected and dried over anhydrous sodium sulfate (Na_2SO_4). Finally, the reduced products were acquired by evaporating the solvent under reduced pressure conditions.

Text S6. Calculation of crystallite size

The crystallite size of Bi_2S_3 nanoparticles was calculated using the Debye-Scherrer formula, which can be expressed as $D = k\lambda/(\beta\cos\theta)$. In this formula, D represents the grain size, λ is the wavelength, k is a shape factor with a value of 0.9, β is the full width at half maximum (FWHM) of the corresponding XRD peak, and θ is the Bragg angle of the most intense peak.

Text S7. Reduction of 4-NP in the presence of molecular H_2 gas

Molecular hydrogen gas (H_2) was employed to reduce 4-NP under ambient conditions. In a typical procedure, 100 ml of a 0.1 mM 4-NP solution was mixed with 20 mg of BS-2 catalyst in a conical flask and stirred for 30 minutes to achieve adsorption-desorption equilibrium. Following this, the solution was continuously purged with H_2 gas for 1h, and time-dependent UV-Vis spectra were recorded to observe changes in 4-NP concentration and the formation of the product 4-AP. However, even after one hour, there was no alteration in the absorption of 4-NP at 317 nm, indicating that molecular H_2 did not reduce 4-NP in the presence of the Bi_2S_3 (BS-2) catalyst under ambient conditions.
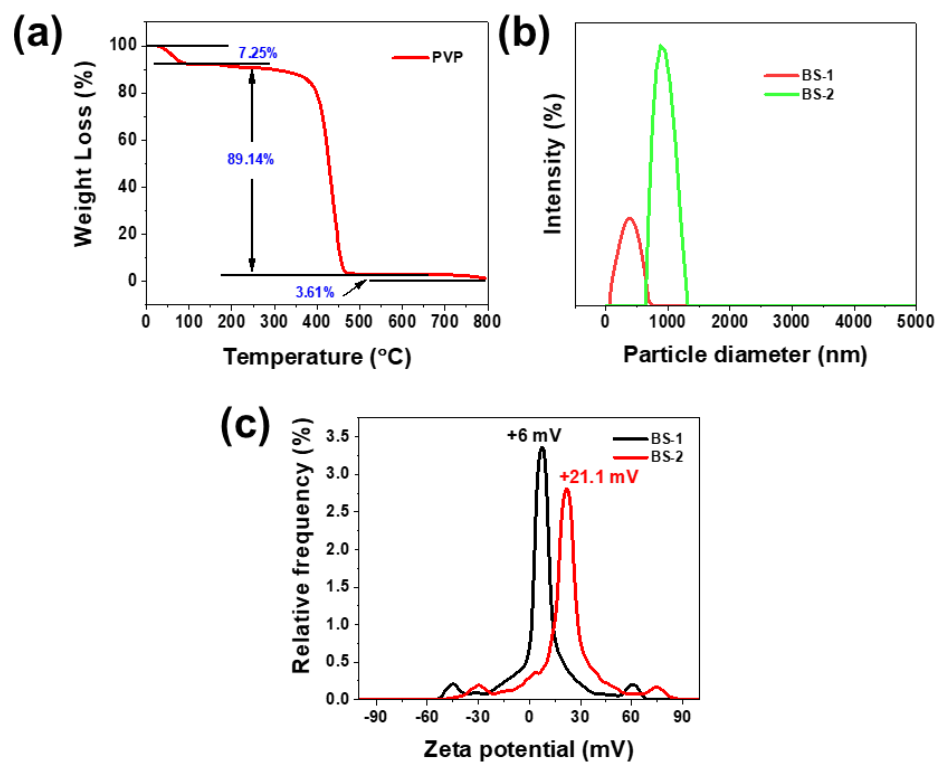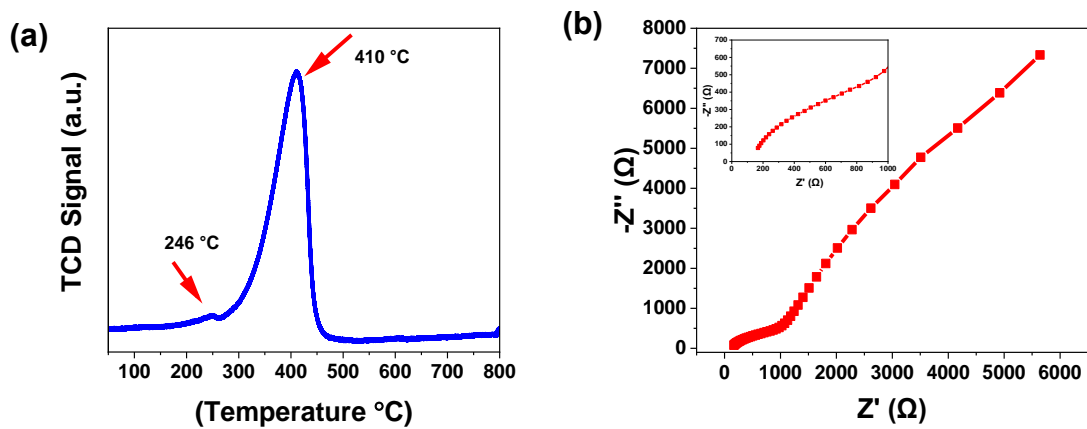
Fig. S1 (a) TGA of PVP; (b)DLS of BS-1 and BS-2; and (c) Zeta potential of BS-1 and BS-2.
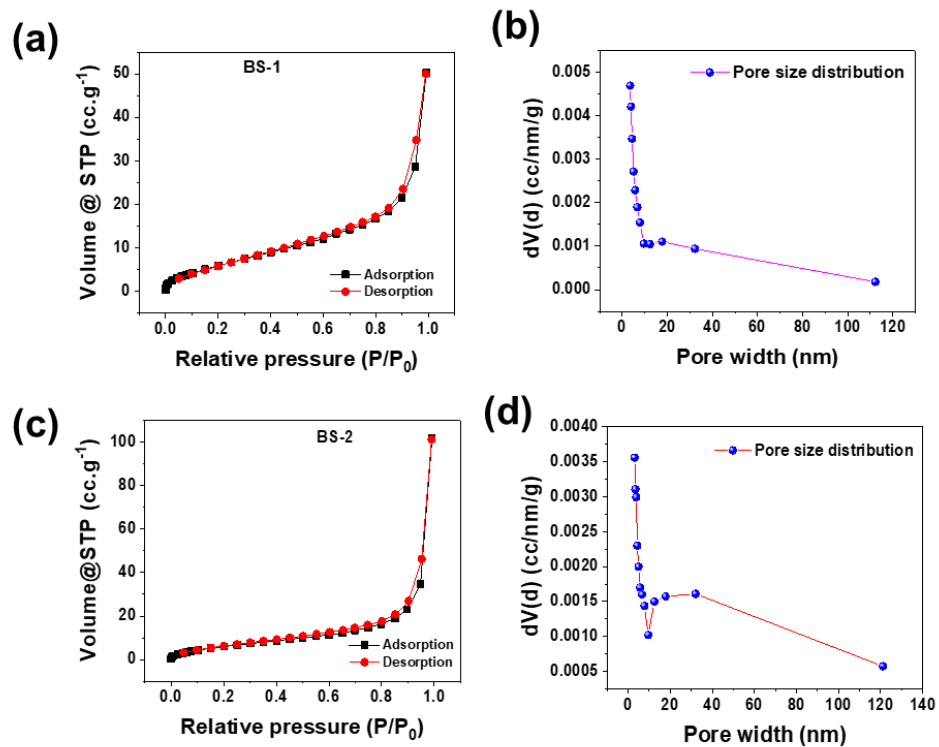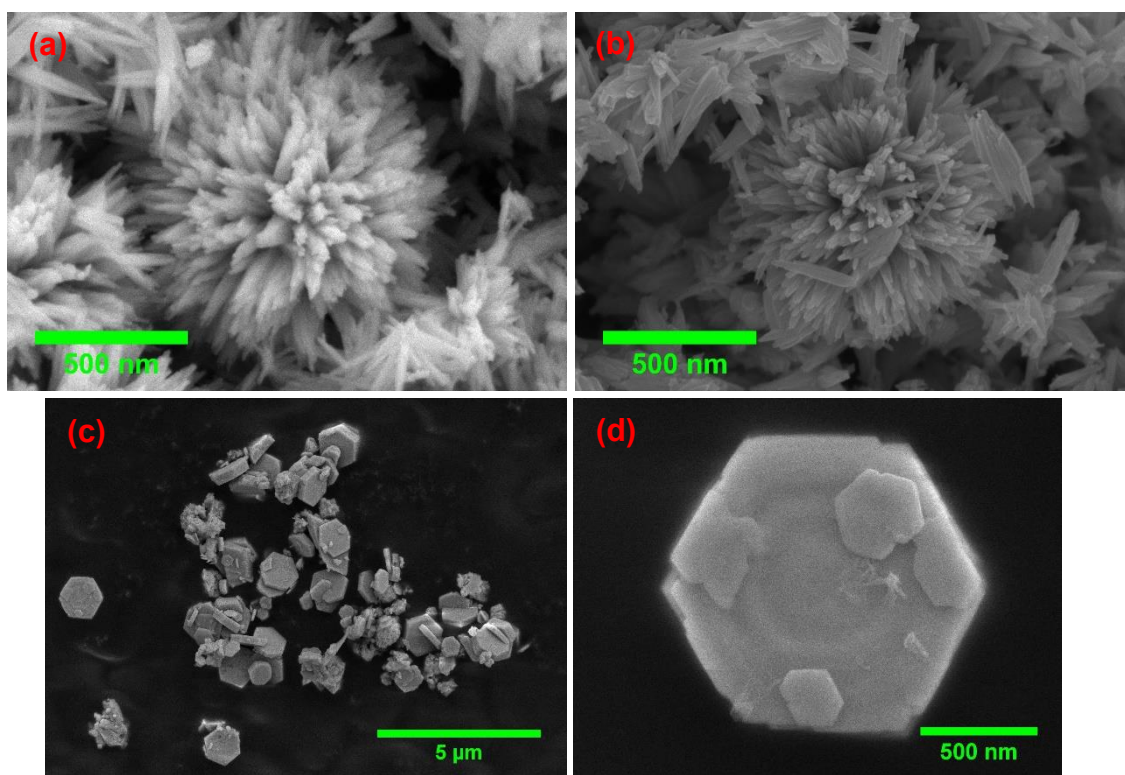
Fig. S2 (a) N$_2$ adsorption-desorption isotherm and (b) BJH pore size distribution of BS-1; (c) N$_2$ adsorption-desorption isotherm and (c) BJH pore size distribution of BS-2.
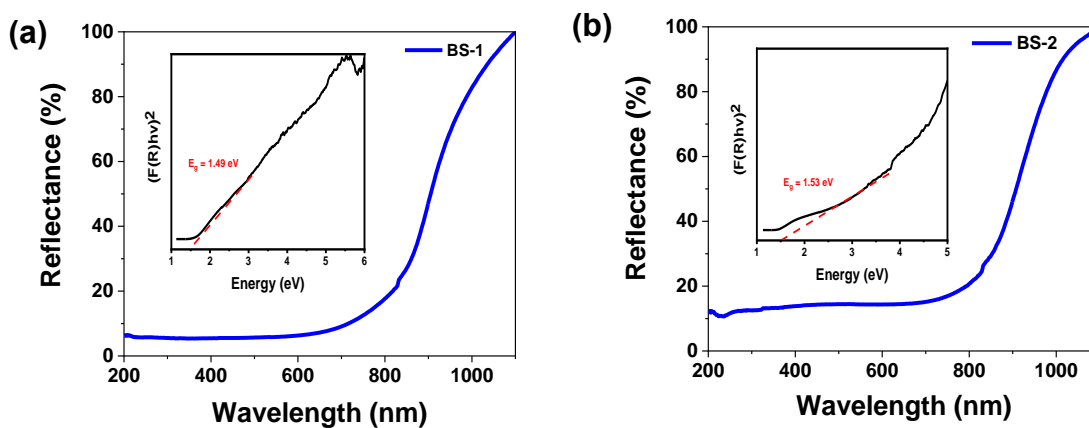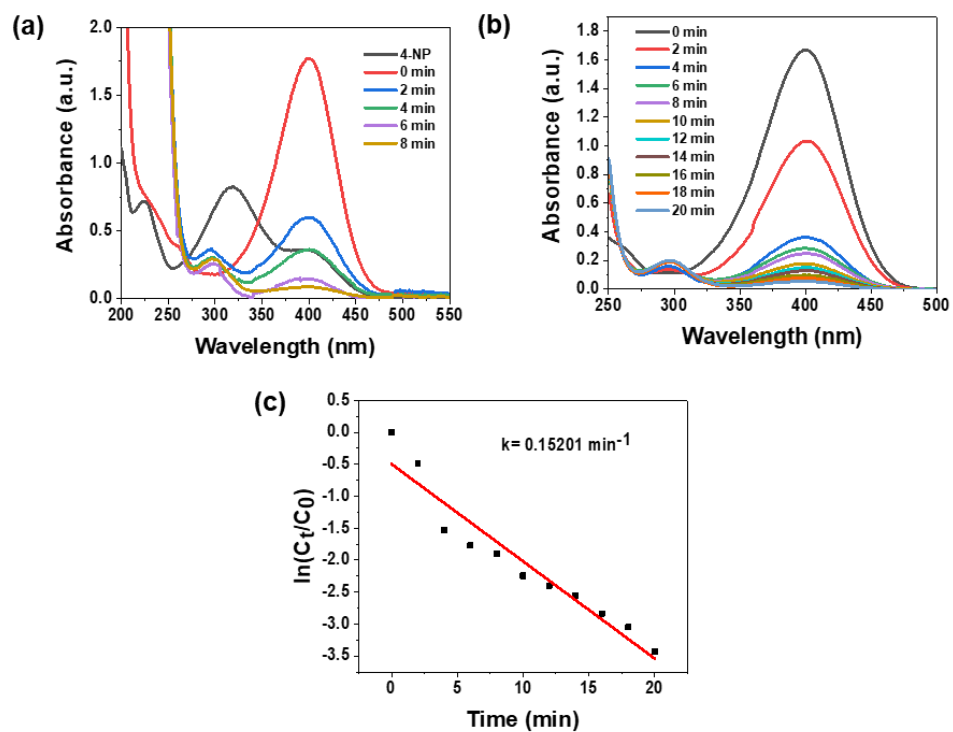

Fig. S3 DRS spectra with inset Kubelka-Munk plot of (a) BS-1 and (b) BS-2.

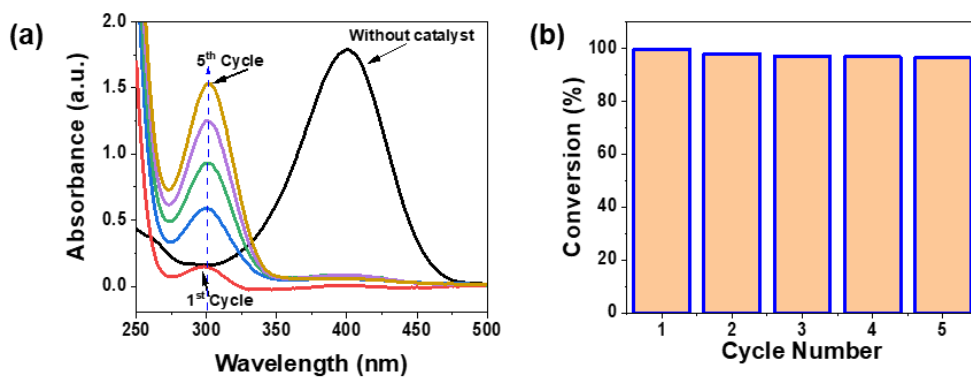**Fig. S4** (a) H$_2$ TPR of BS-2 and (b) Nyquist plot of BS-2.

Fig. S5 FE-SEM micrographs of (a) BS-1 SE2 mode; (b) BS-1 InLens mode, (c) and (d) of BS-2 in SE2 modes.

Fig. S6 UV-Vis spectra of 4-NP reduction(a) in the presence of BS-2; (b) in the presence of BS-1; and (c) plot of $\ln(C_t/C_0)$ vs time for BS-1. (Conditions: [4-NP] = 76.9 µM, [NaBH$_4$] = 20.3 mM, [Cat] = 0.2 g/L).

Fig. S7 (a) Time-dependent UV-Vis spectra of 4-NP reduction by BS-2 for 5 cycles, (b) Conversions at the end of each cycle. (Initial Conditions: [4-NP] = 76.9 µM, [NaBH$_4$] = 20.3 mM, [Cat] = 0.2 g/L).
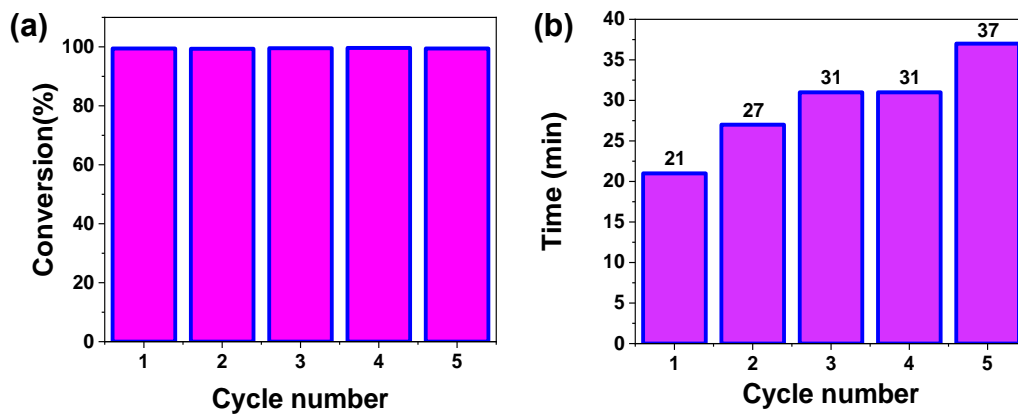
Fig. S8 (a) Reusability of BS-2 for the reduction of 4-NP and (b) required time for each cycle for the complete reduction of 4-NP by BS-2. (Conditions: [4-NP] = 5 mM, [NaBH$_4$] = 44.1 mM, [Cat] = 0.8 g/L).

Table S1 Comparison of catalytic activities of different bismuth-based catalysts for 4-NP reduction.

Catalyst	K_{nor}	Ref.
Bi_2S_3@quasi-Bi-MOF	435298 s^{-1} g^{-1}	[1]
Bismuth nanodots	6.033 s^{-1} g^{-1}	[2]
BiNPs	9.87 $min^{-1}g^{-1}$	[3]
Bi NPs	27.51 s^{-1} g^{-1}	[4]
Bi NPs/N-doped Graphene	32.1 min^{-1} mg^{-1}	[5]
BiNPs	0.1 s^{-1} g^{-1}	[6]
Bi@Cs	242.9 s^{-1} g^{-1}	[7]
Bi_2S_3	323 min^{-1} g^{-1}	[8]
QTMC-BiNPs	25.42 s^{-1} g^{-1}	[9]
Au/Bi_2Se_3 nanosheets	386.67 $s^{-1}g^{-1}$	[10]
1D-2D Bi_2S_3	**52920 s^{-1} g^{-1}** **(882 min^{-1} g^{-1})**	**This work**

Table S2 Thermodynamic parameters for 4-NP reduction using BS-2 at different temperatures.

| Temperature (K)	E_a (kJ/mol)	$\Delta H^{\#}$ (kJ/mol)	$\Delta S^{\#}$ (J/mol K^{-1})	$\Delta G^{\#}$ (kJ/mol)
283	26.13	23.66	-171.48	72.19
293				73.90
303				75.62
313				77.33
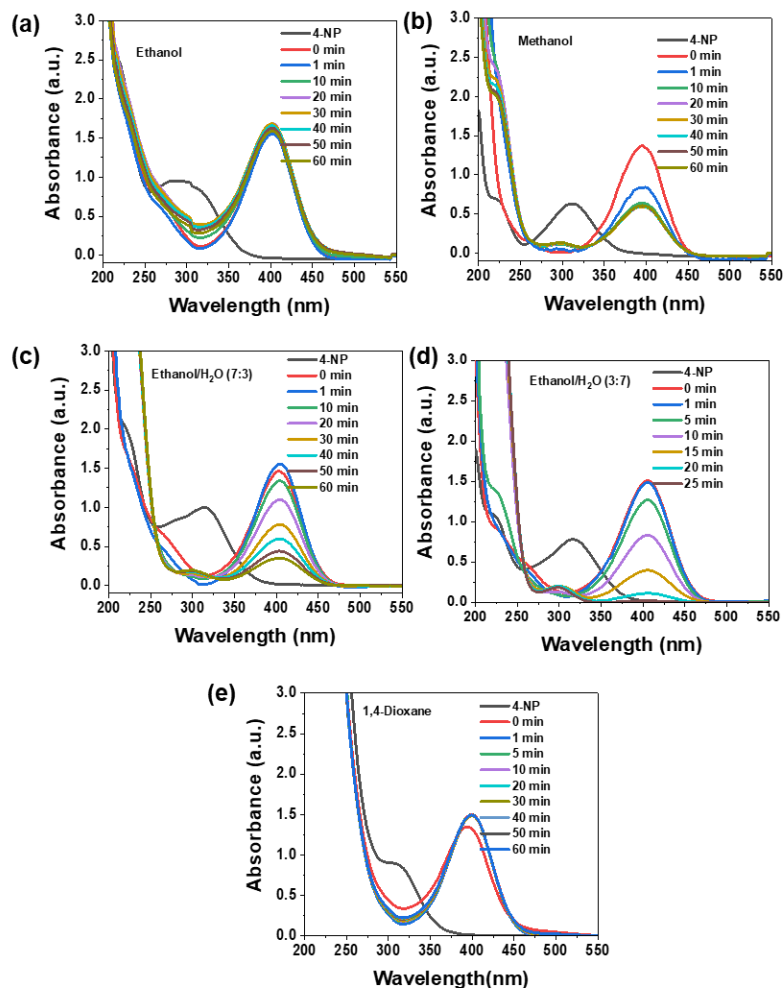
Fig. S9 Time-dependent UV-Vis spectra of 4-NP reduction by BS-2 in solvent (a) ethanol, (b) methanol, (c) Ethanol/ H_2O (7:3), (d) Ethanol/H_2O (3:7), and (e) 1,4 dioxane. (Conditions: [4-NP] = 76.9 µM, [$NaBH_4$] = 20.3 mM, [Cat] = 0.2 g/L).

Table S3 Effects of solvent on reduction of 4-nitrophenol over 1D-2D Bi_2S_3 (BS-2).

Solvent	Reaction time (min)	Conversion (%)
Ethanol	60	0
Methanol	60	60
H_2O	8	100
Ethanol/ H_2O (7:3)	60	77
Ethanol/H_2O (3:7)	25	100
1,4-Dioxane	60	0

Reaction conditions: 0.2 ml of 1mM 4-nitrophenol aqueous solution; 0.053 mmol $NaBH_4$; 2.3 ml of various solvents.
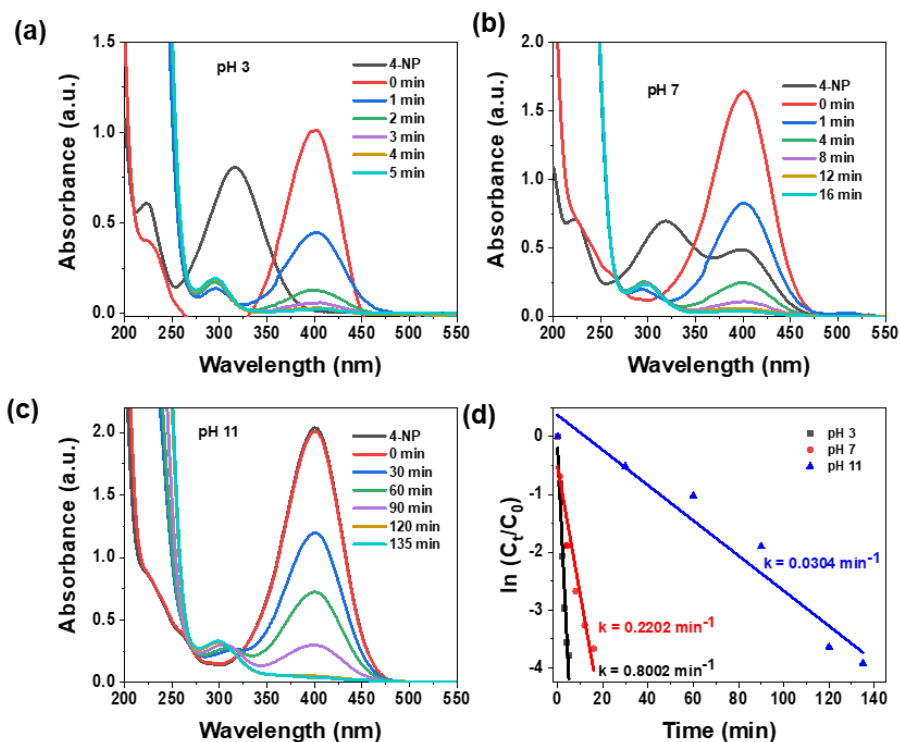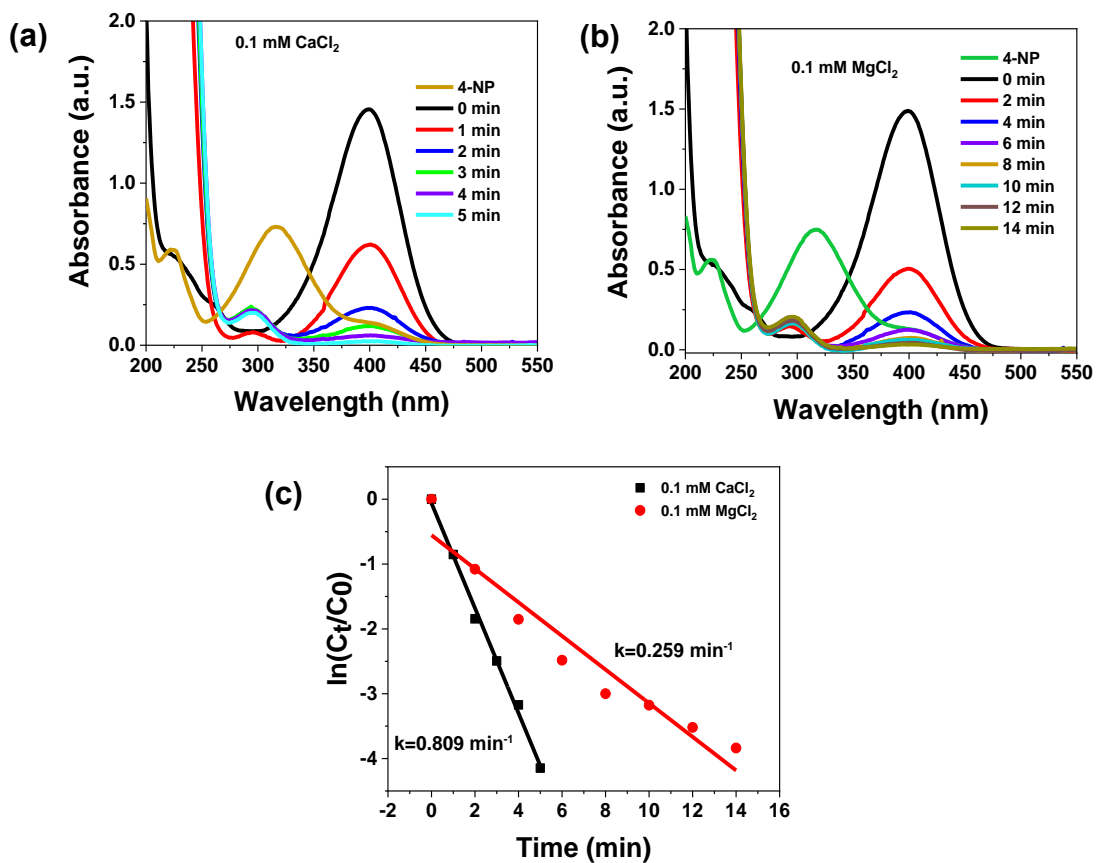

Fig. S10 Time-dependent UV-vis spectra of 4-NP reduction by BS-2 at initial pH of 4-NP solution (a) pH 3, (b) pH 7, (c) pH 11, and (e) $\ln(C_t/C_0)$ vs time plot. (Conditions: [4-NP] = 76.9 μM, [$NaBH_4$] = 20.3 mM, [Cat] = 0.2 g/L).
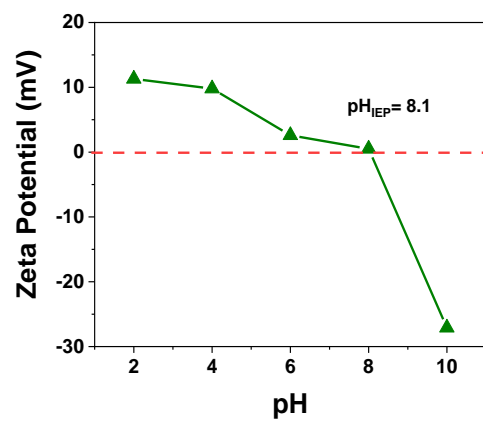
Fig. S11 pHIEP of BS-2.
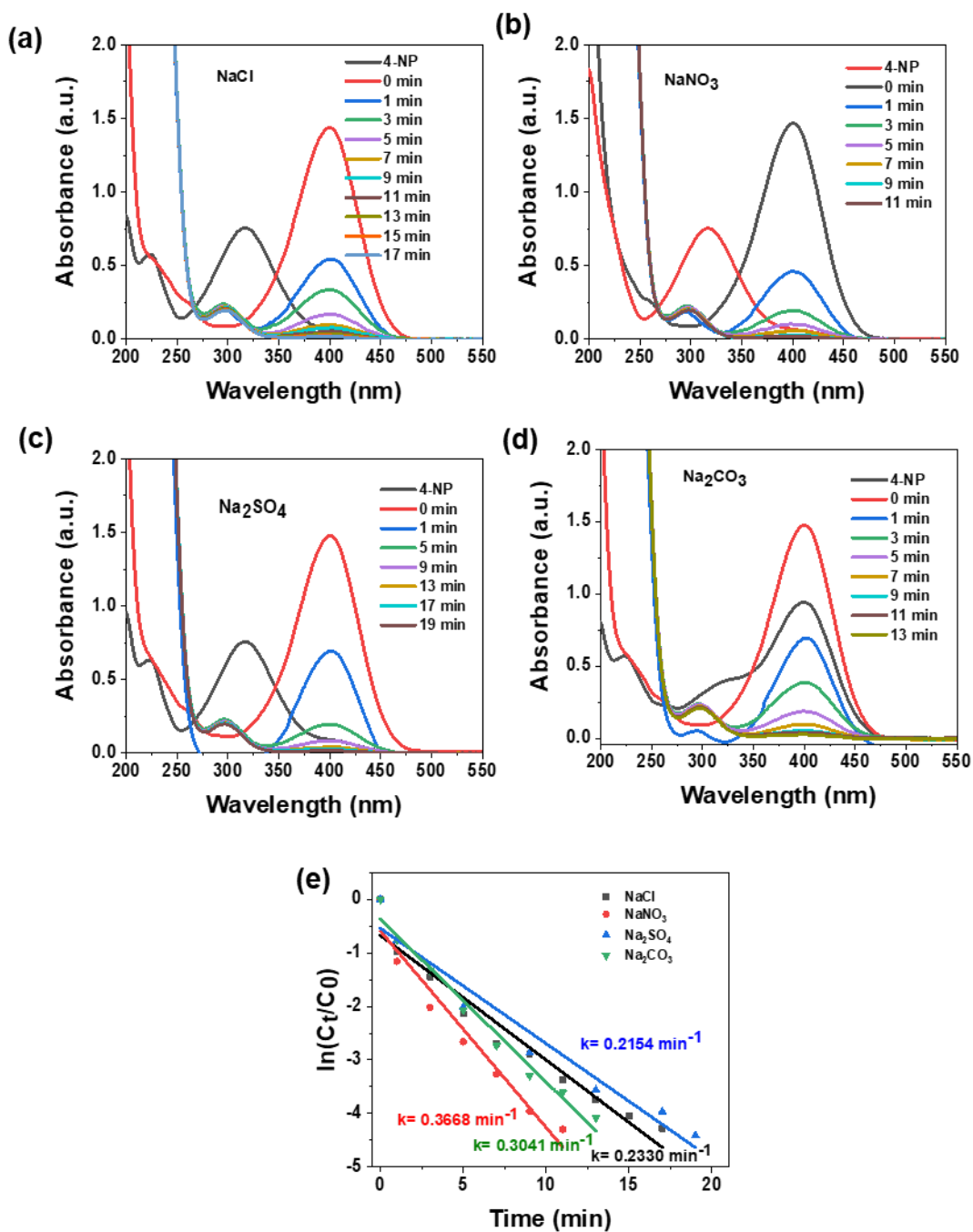
Fig. S12 Time-dependent UV-Vis spectra of 4-NP reduction by BS-2 in the presence of anions (a) Cl⁻, (b) NO_3^-, (c) SO_4^{2-}, (d) CO_3^{2-}, and (e) $\ln(C_t/C_0)$ vs time plot. (Conditions: [4-NP] = 76.9 μM, [NaBH₄] = 20.3 mM, [Cat] = 0.2 g/L, [anion] = 0.1 mM).

Fig. S13 Time-dependent UV-Vis spectra of 4-NP reduction by BS-2 in the presence of cations (a) Ca^{2+}, (b) Mg^{2+}, and (c) $\ln(C_t/C_0)$ vs time plot. (Conditions: [4-NP] = 76.9 µM, [$NaBH_4$] = 20.3 mM, [Cat] = 0.2 g/L & [Cation] = 0.1 mM).
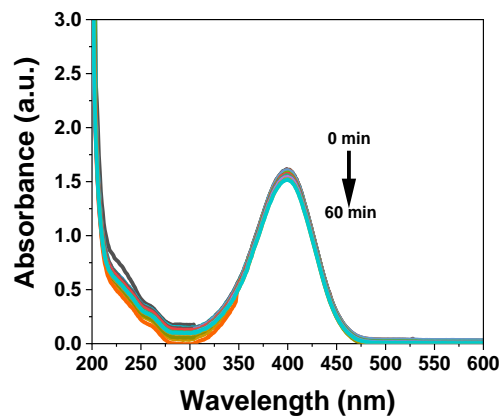
Fig. S14 Time-dependent UV-Vis spectra of reduction of 4-NP using Ca^{2+} and $NaBH_4$ without the use of catalyst. (Conditions: [4-NP] = 76.9 µM, & [$NaBH_4$] = 20.3 mM).
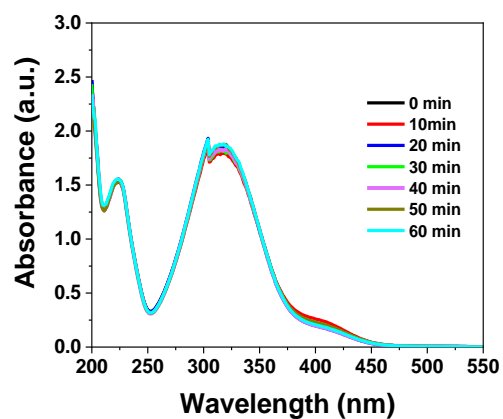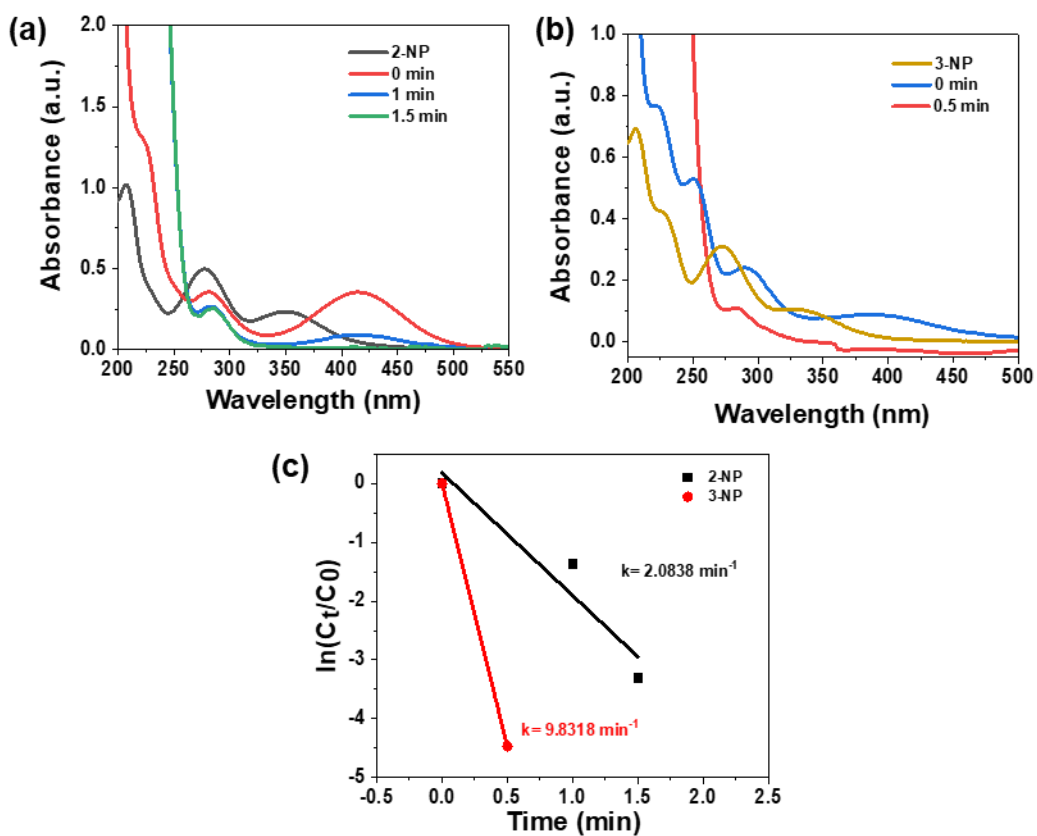

Fig. S15 Time-dependent UV-Vis spectra for BS-2 catalyst assisted 4-NP reduction in the presence of molecular H_2 gas. (Conditions: [4-NP] = 0.1 mM, & [Cat] = 0.2 g/L).
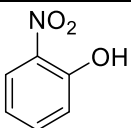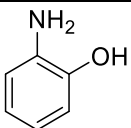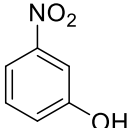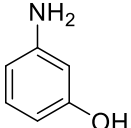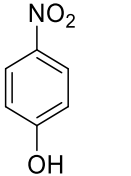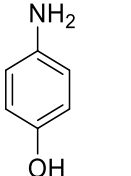
Table S4 Zeta potentials of the reaction solution in the presence of Bi_2S_3 and different common anions.

Common anions	None	Na_2SO_4	NaCl	$NaNO_3$	Na_2CO_3
Zeta potential (mV)	-17.6	-14.8	-23.0	-17.1	-13.1
Conditions: [4-NP] = 76.9 µM, [NaBH₄] = 20.3 mM, [Cat] = 0.2 g/L, [anion] = 0.1 mM.					

Fig. S16 Time-dependent UV-Vis spectra of reduction of (a) 2-NP, (b) 3-NP, and (c) $\ln(C_t/C_0)$ vs. t plots. (Conditions: [4-NP] = 76.9 µM, [NaBH₄] = 20.3 mM, [Cat] = 0.2 g/L).

Table S5 Catalytic Reduction Activity of Diverse Nitroarenes by the BS-2.

Entry	Substrate	Product	Time (min)	TOF (h^{-1})
1	NO$_2$ ... OH	NH$_2$ ... OH	1.5	8.2305
2	NO$_2$ ... OH	NH$_2$ ... OH	0.5	24.6913
3	NO$_2$ ... OH	NH$_2$ ... OH	8	1.5432
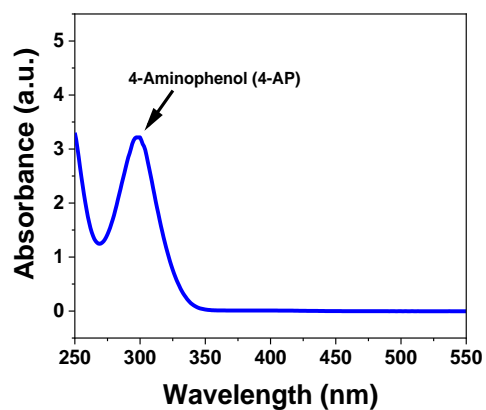
Fig. S17 Product confirmation from large scale reduction of 4-NP.
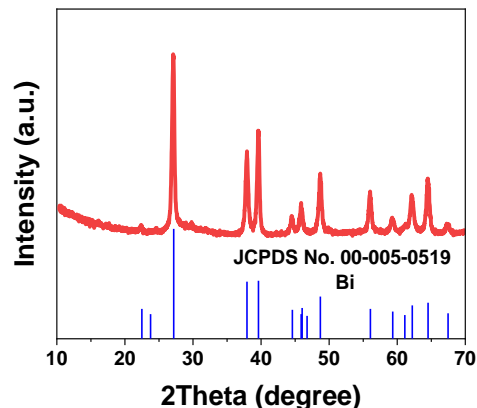
Fig S18. P-XRD pattern of BS-2 catalyst after introducing $NaBH_4$ to BS-2 without the 4-NP.

Calculation of turnover number (TON) and turnover frequency (TOF) of 4-nitrophenol to 4-aminophenol catalyzed by 1D-2D Bi_2S_3

The efficacy of a catalyst for 4-nitrophenol reduction can be determined by the turnover number (TON) and turnover frequency (TOF). TON is calculated using number of moles of substrate convert into products per mole of catalyst.

$$TON = \frac{\text{Number of moles of 4-NP reduced to 4-AP}}{\text{Number of moles of catalyst}}$$

TOF is defined as the number of moles of 4-NP reduced to 4-AP per mole of catalyst per hour. It is calculated by dividing TON by reaction time.

$$TOF \ (h^{-1}) = \frac{TON}{\text{Reaction time (in h)}}$$

In other words,

$$TOF \ (h^{-1}) = \frac{\text{Number of moles of 4-NP reduced to 4-AP}}{\text{Number of moles of catalyst} \times \text{reaction time (h)}}$$

19

Moles of conversion of 4-NP to 4-AP = $C_{4-NP} * V_{4-NP}$

Where C_{4-NP} = molar concentration of 4-NP (1mM or 1mmol/L)

V_{4-NP} = Volume of 4-NP (200 µl)

∴ Moles of 4-NP to 4-AP = 1 mmol/L * 200 µl

$$= 2 \times 10^{-7} \text{ moles}$$

No. of Moles of catalyst $= \dfrac{\text{Mass concentration of Bi}_2\text{S}_3 \times \text{Volume of Bi}_2\text{S}_3}{\text{Relative molecular mass of Bi}_2\text{S}_3}$

Mass concentration of Bi_2S_3 = 5 mg/ml

Volume of Bi_2S_3 taken = 100 µl

Relative molecular mass of Bi_2S_3 = 514.16 g/mol

∴ Moles of Bi_2S_3 = (5 mg/ml * 100 µl)/514.16 g/mol

$$= 9.72 \times 10^{-7} \text{ moles}$$

$$\text{TON} = \frac{2 \times 10^{-7} \text{ moles}}{9.72 \times 10^{-7} \text{ moles}} = 0.2057$$

TOF (h^{-1}) = 0.2057/ 8 min^{-1} = 0.02571 min^{-1} = 1.543 h^{-1}

Table S6: Comparison of thermodynamic parameters for 4-NP reduction presented in literatures and this work.

Samples	E_a (kJ mol^{-1})	$\Delta H^{\#}$ (kJ mol^{-1})	$\Delta S^{\#}$ (J mol^{-1} K^{-1})	$\Delta G^{\#}$ (kJ mol^{-1})	References
Bi/N-doped Graphene	29.1	-	-	-	[5]
20% Bi_2S_3/$NiCo_2O_4$	26.27	25.02	-197.46	83.86 (at 298 K)	[8]
1D-2D Bi_2S_3	26.13	23.66	-171.48	72.19 (at 283K)	**This work.**
				73.90 (at 293K)	
				75.62 (at 303K)	
				77.33 (at 313K)	

References:

[1] J. Jiang, W. Wei, Y. Tang, S. Yang, X. Wang, Y. Xu, L. Ai, In Situ Implantation of Bi_2S_3 Nanorods into Porous Quasi-Bi-MOF Architectures: Enabling Synergistic Dissociation of Borohydride for an Efficient and Fast Catalytic Reduction of 4-Nitrophenol, Inorg. Chem., 61 (2022) 19847-19856.

[2] Y. Liang, J. Manioudakis, J.-R. Macairan, M.S. Askari, P. Forgione, R. Naccache, Facile aqueous-phase synthesis of an ultrasmall bismuth nanocatalyst for the reduction of 4-nitrophenol, ACS omega, 4 (2019) 14955-14961.

[3] M. Mahiuddin, B. Ochiai, Comprehensive study on lemon juice-based green synthesis and catalytic activity of bismuth nanoparticles, ACS omega, 7 (2022) 35626-35634.

[4] F. Xia, X. Xu, X. Li, L. Zhang, L. Zhang, H. Qiu, W. Wang, Y. Liu, J. Gao, Preparation of bismuth nanoparticles in aqueous solution and its catalytic performance for the reduction of 4-nitrophenol, Ind. Eng. Chem. Res., 53 (2014) 10576-10582.

[5] S. Li, Y. Yang, L. Liu, Q. Zhao, Electron transfer-induced catalytic enhancement over bismuth nanoparticles supported by N-doped graphene, J. Chem. Eng., 334 (2018) 1691-1698.

[6] M. Mahiuddin, B. Ochiai, Green synthesis of crystalline bismuth nanoparticles using lemon juice, RSC Adv., 11 (2021) 26683-26686.

[7] J. Zhou, J. Gao, X. Xu, W. Hong, Y. Song, R. Xue, H. Zhao, Y. Liu, H. Qiu, Synthesis of porous Bi@ Cs networks by a one-step hydrothermal method and their superior catalytic activity for the reduction of 4-nitrophenol, J. Alloys Compd., 709 (2017) 206-212.

[8] F.M. Valadi, E. Akbarzadeh, M.R. Gholami, Efficient reduction of organic pollutants by novel magnetic $Bi_2S_3/NiCo_2O_4$ MOF-derived composite: Exprimental and DFT investigation, J. Mol. Liq., 367 (2022) 120574.

[9] Y.A. Alli, S. Adewuyi, B.S. Bada, S. Thomas, H. Anuar, Quaternary trimethyl chitosan chloride capped bismuth nanoparticles with positive surface charges: catalytic and antibacterial activities, J. Clust. Sci., 33 (2022) 2311-2324.

[10] L. Xiao, A. Zhu, Q. Xu, Y. Chen, J. Xu, J. Weng, Colorimetric biosensor for detection of cancer biomarker by Au nanoparticle-decorated Bi_2Se_3 nanosheets, ACS Appl. Mater. Interfaces. , 9 (2017) 6931-6940.